Catalytic hydrogen evolution by Fe(II) carbonyls featuring a dithiolate and a chelating phosphine

*Souvik Roy[†§‡], Shobeir K. S. Mazinani[†§], Thomas L. Groy[†], Lu Gan[†§], Pilarisetty Tarakeshwar[†], Vladimiro Mujica[†§], Anne K. Jones[†§]**

[†]Department of Chemistry and Biochemistry; [§]Center for Bio-Inspired Solar Fuel Production, Arizona State University, Tempe, AZ 85287, USA

*To whom correspondence should be addressed

e-mail: jonesak@asu.edu

Tel: 480-965-0356

[‡]Current Address: Dr. Souvik Roy, Laboratoire de Chimie et Biologie des Métaux, CEA-Grenoble, 17 rue des Martyrs, 38054 Grenoble Cedex 9, France

Abstract:

Two pentacoordinate mononuclear iron carbonyls of the form (bdt)Fe(CO)P_2 [bdt = benzene-1,2-dithiolate; P_2 = 1,1'-diphenylphosphinoferrocene (**1**) or methyl-2-{bis(diphenylphosphinomethyl)amino}acetate (**2**)] were prepared as functional, biomimetic models for the distal iron (Fe_d) of the active site of [FeFe]-hydrogenase. X-ray crystal structures of the complexes reveal that, despite similar ν(CO) stretching band frequencies, the two complexes have different coordination geometries. In X-ray crystal structures, the iron center of **1** is in a distorted trigonal bipyramidal arrangement, and that of **2** is in a distorted square pyramidal geometry. Electrochemical investigation shows that both complexes catalyze electrochemical proton reduction from acetic acid at mild overpotential, 0.17 and 0.38 V for **1** and **2**, respectively. Although coordinatively unsaturated, the complexes display only weak, reversible binding affinity towards CO (1 bar). However, ligand centered protonation by the strong acid, $HBF_4.OEt_2$, triggers quantitative CO uptake by **1** to form a dicarbonyl analogue **[1(H)-CO]**$^+$ that can be reversibly converted back to **1** by deprotonation using NEt_3. Both crystallographically determined distances within the bdt ligand and DFT calculations suggest that the iron centers in both **1** and **2** are partially reduced at the expense of partial oxidation of the bdt ligand. Ligand protonation interrupts this extensive electronic delocalization between the Fe and bdt making **1(H)**$^+$ susceptible to external CO binding.

Introduction

Hydrogen produced from solar energy and water offers the tantalizing opportunity to produce a storable, renewable fuel on a scale comparable to global energy challenges.[1] However, developing efficient and renewable catalysts for this transformation has proven challenging. Thus hydrogenases, the biological catalysts for reversible proton reduction to hydrogen, have caught the attention of a broad range of researchers.[2, 3] Since the elucidation of the structures of both [NiFe]- and [FeFe]-hydrogenases revealed that these enzymes feature organometallic active sites including the diatomic ligands CO and CN (Figure 1),[4-7] inorganic chemists have sought to produce both structural and functional models in an effort to understand and reproduce these enzymes.[8] However, although natural hydrogenases have turnover frequencies exceeding 1000 s^{-1} at potentials close to the thermodynamic reduction potential of the proton, synthetic models seldom come close to this exquisite reactivity.[9, 10]

The active site of [FeFe]-hydrogenases, referred to as the H-cluster, is a unique six iron cluster consisting of a [4Fe4S] cluster bridged *via* a cysteinyl thiolate to a diiron subsite.[5, 6] This diiron subcluster, although biologically unprecedented, is highly reminiscent of known organometallic complexes. As shown in Figure 1, it consists of a dithiolate ligand bridging the two iron ions as well as the strong π-acceptors CO and CN^- at each iron center. The proximal iron, Fe_p, so designated due to its relative proximity to the [4Fe4S] center, is a coordinatively saturated, octahedral site. On the other hand, hydrogen binding or production occurs at the distal iron, Fe_d, an electron deficient, five-coordinate, pseudo-square pyramidal center featuring a terminal open coordination site.

Organometallic complexes of the type $[(\mu\text{-}SR_2)Fe_2(CO)_6]$ and their derivatives in which one or more of the carbonyls have been replaced with more strongly σ-donating ligands such as phosphines, have been used extensively as both structural and functional mimics of [FeFe]-hyrogenases.[3, 11, 12] Although the natural enzyme features iron centers in square pyramidal environments that are inverted relative to each other such that a terminal open coordination site is available, the irons in most of these model complexes are in the so-called "eclipsed" geometry in which the two pyramids have the same orientation. Complexes with an "inverted" iron center, although known, remain the exception.[13-15] In an eclipsed geometry, the bridging, as opposed to terminal, position is most reactive, facilitating formation of stable but unreactive bridging hydrides.[16-18] Thus the models tend to be poor catalysts for proton reduction and require substantial overpotentials for the catalysis. Development of mononuclear iron complexes with an open coordination site can, in principle, overcome this difficulty and mimic the reactivity of the distal iron site of the enzyme if an appropriate ligand set can be found to simulate the electronic environment of the second missing metal.

Although synthetic efforts immediately following the elucidation of the crystal structure of [FeFe]-hydrogenases produced a series of coordinatively saturated mononuclear iron complexes as spectroscopic models for the H-cluster,[19-21] relatively few five coordinate models have been reported. Liaw and coworkers demonstrated the synthesis of a pentacoordinate, 16-electron Fe(II) complex $[Fe(CO)_2(CN)(S,NH\text{-}C_6H_4)]^-$ and showed that it readily reacted to form hexacoordinate complexes or dimers.[22] They did not, however, investigate the catalytic activity of this compound. Darensbourg and coworkers have also produced pentacoordinate iron dicarbonyls using the strongly π-

donating, redox noninnocent ligand 2-amido-thiophenylate as models for the mononuclear Fe-containing hydrogenases.[23, 24] Particularly relevant to this work, Sellmann and coworkers employed the benzene-1,2-dithiolate (bdt) ligand to construct $[Fe(bdt)(PMe_3)_2(CO)_2]$ and noted that it had an unexpected tendency to lose CO to form a 16 electron complex.[25] Rauchfuss and coworkers used that work as an inspiration to create $(Et_4N)_2[Fe(bdt)(CN)_2(CO)]$, as a spectroscopic model of the enzyme active site.[26] Only recently did Ott and coworkers report complexes of bdt together with a chelating phosphine to create coordinatively unsaturated monocarbonyl models of the distal iron site of [FeFe]-hydrogenases and to show that these compounds are active in electrocatalytic proton reduction.[27-29]

In this paper, we present a new coordinatively unsaturated, five-coordinate Fe(II)-carbonyl in a P_2S_2 coordination environment. The phosphines are provided by 1,1'-{bis(diphenyl)phosphino}ferrocene (dppf), and the steric constraints of the ferrocene moiety in this ligand cause it to have one of the largest bite angles observed for a chelating phosphine. On the other hand, benzene-1,2-dithiolate (bdt), well known for its redox activity associated with the conjugation of the sulfur donors to the aromatic ring, provides the sulfur ligands. The result is that $[(\kappa^2\text{-dppf})Fe(CO)(\kappa^2\text{-bdt})]$ (**1**) **e**lectrocatalytically reduces protons from the weak acid acetic acid with unprecedentedly low overpotentials. Furthermore, the protonated complex binds exogenous CO, a reaction seldom seen in model compounds but well known for the enzyme. The electrocatalytic properties of this complex are directly compared to those of an analogous compound $[(\kappa^2\text{-}NP_2)Fe(CO)(\kappa^2\text{-bdt})]$ (**2**) for NP_2 = methyl-2,-{bis(diphenylphosphinomethyl)amino}acetate, and electronic explanations for the

differing reactivities of the two pentacoordinate complexes based on density functional theory (DFT) calculations are considered.

Results

Synthesis and spectroscopic characterization. Two pentacoordinate iron(II)-carbonyl complexes each with a chelating bis-phosphine and benzene-1,2-dithiol (bdt) were synthesized starting from $FeCl_2$: (κ^2-dppf)Fe(CO)(κ^2-bdt) (**1**) and (κ^2-NP_2)Fe(CO)(κ^2-bdt) (**2**) where dppf is 1,1'-bis(diphenylphosphino)ferrocene and NP_2 is methyl-2-{bis(diphenylphosphinomethyl)amino}-acetate (Scheme 1). The bdt ligand was employed both for its strong π-donor propensity and its redox activity. Similarly, dppf was chosen because it is chelating and, among common chelating bis-phosphine ligands, has one of the widest bite angles. This angle has a major influence on the structure of the resulting complex and the corresponding catalytic properties.[30-33] For comparison, to evaluate the impact of dppf on the electronic and catalytic properties of the $Fe^{II}S_2P_2$ center, **2**, which features an N-containing bis-phosphine ligand (NP_2) instead of dppf, was synthesized. The ligand NP_2 is easily obtained by reaction of two equivalents of Ph_2PCH_2OH with glycine methyl ester in refluxing ethanol.[34] As shown in Scheme 1, treatment of a methanolic solution of anhydrous $FeCl_2$ with a solution of the appropriate bis-phosphine in THF and benzene-1,2-dithiol in the presence of a base (triethylamine) under a CO atmosphere afforded the desired diamagnetic complexes, **1** and **2**, in 65% and 60% isolated yields, respectively. A single resonance is observed in the $^{31}P\{^1H\}$ NMR spectrum at 66.32 ppm for **1** and 50.21 ppm for **2** (^1H NMR spectra are available in supplementary information).

In a tetrahydrofuran (THF) solution, **1** is reddish brown with visible absorbances at 467 nm (ε = 4433 $M^{-1}\,cm^{-1}$) and 745 nm (ε = 974 $M^{-1}\,cm^{-1}$) (Figure 2). Another very

intense band in the UV range 250–300 nm arising from the π-π* transition of the phenyl groups was also present. The 467 nm band features a prominent shoulder on the lower energy side, and, by comparison to the spectrum of **2** (vide infra) likely consists of two distinct charge transfer transitions. The 745 nm band is thought to arise from a d-d transition. By comparison, despite a similar coordination environment and metal oxidation state, **2** is dark green in a THF solution with absorption maxima at 437 nm (ε = 4537 M^{-1} cm^{-1}) and 579 nm (ε = 2883 M^{-1} cm^{-1}). These bands are tentatively assigned as charge transfers involving the Fe center and the benzene-1,2-dithiolate ligand.

IR spectra of both **1** and **2** in dichloromethane consist of a single peak in the CO-stretching region at 1918 or 1915 cm^{-1}, respectively (Figure 3A and 3B, grey traces). The energy of this absorbance is comparable to that of related Fe^{II} complexes such as (κ^2-dppp)Fe(CO)(Cl_2bdt) (dppp = diphenylphosphinopropane, Cl_2bdt = 3,6-dichloro-1,2-benzenedithiolate).[27] The remarkable similarity of the CO-stretching frequencies for the two complexes indicates that changing the bis-phosphine ligand has little detectable impact on the Fe-CO bonding interactions.

Crystal Structures. The structures of **1** and **2** were determined by single-crystal X-ray diffraction and are shown in Figure 4. Selected bond distances and angles are given in Tables 1 and 2, and additional crystallographic information is available in Table S1. Crystals were grown by slow diffusion of hexane into a dichloromethane (**1**) or chloroform (**2**) solution of complex. The two complexes feature remarkably different geometries about the central iron atom. Complex **2** is a distorted square pyramid (SP) with an axial CO ligand while complex **1** is a distorted trigonal bipyramid (TBP) with CO, phosphorus and sulfur in the equatorial positions and phosphorus and sulfur in the

apical positions. The geometries of the complexes were further characterized by Addison's τ value, defined as $\tau=(\beta-\alpha)/60$ for which β is the larger of the angles between the *trans* ligands on the basal plane of a SP or the angle between the two axial ligands for a TBP. The parameter α is defined as the smaller of the angles between the *trans* ligands on the basal plane of a SP or the larger of the basal angles for a TBP.[35] For pentacoordinate complexes, τ is a measure of the degree of distortion from ideal SP (τ = 0) or ideal TBP (τ = 1) geometry. The calculated value of τ is 0.099 for **2** (based on β(S1-Fe1-P2) = 165.1427˚ and α(S2-Fe1-P1) = 159.2057˚) and 0.721 for **1** (based on β(S2-Fe1-P1) = 171.7433˚ and α(S1-Fe1-P2) = 128.4776˚) corroborating the geometric assignments of the complexes. As noted above, dppf has a much larger bite-angle (P-Fe-P = 101.17˚) than NP_2 (87.49˚), and this difference is likely responsible for the geometric differences about the irons of **1** and **2**. For complex **1**, the three equatorial ligands show a significant distortion from C_3 symmetry with bond angles of 134.58˚ (C-Fe-S), 128.48˚ (S-Fe-P), and 96.69˚ (P-Fe-C). The two axial ligands, thiolate and phosphine, are also slightly distorted from a linear arrangement with an S-Fe-P angle of 171.74˚. We note that **1** is a diamagnetic, formally Fe^{II} complex. Perfect TBP geometry does not permit a diamagnetic ground state for a d^6 metal, but the observed distorted geometry is consistent with the S = 0 ground state.[36, 37] It is also worth noting that the coordination geometry may be different in solution. Despite the metal coordination geometry differences, the Fe-C and C-O bond lengths of **1** and **2** are very similar to each other. This is consistent with the similar ν(CO) stretching frequencies observed for the two complexes. Additionally, as shown in Table 2, the C-C bond lengths of the benzene-1,2-dithiolato ligand show an alternating pattern of two shorter C-C bonds (average 1.37 Å for **1** and 1.38 Å for **2**) and

four longer ones (average 1.40 Å for **1** and **2**) for both **1** and **2**. Moreover, the two C-S bonds are also not identical. The average C-S bond lengths, 1.74 Å for **1** and 1.75 Å for **2,** are slightly shorter than typical bond lengths for the C-S single bonds (1.76 - 1.77 Å) in benzene-1,2-dithiolate, suggesting that in the metallocomplexes the C-S bond orders are greater than one.[38-40] The observed distortions of the bdt ligand represent clear evidence that it is partially oxidized and possesses substantial 1,2-dithiobenzosemiquinonate, π-radical character.[40] Concomitantly, the charge of the Fe center in both complexes is expected to be less than +2 (see computational studies below). The distortion of the ligand is more obvious for **1** indicating that the bdt ligand is more oxidized and the pentacoordinate Fe center is more reduced in this complex than in **2**.

Reactivity towards CO. To investigate whether the open coordination site on complexes **1** and **2** is accessible for external ligand binding, reactions of **1** and **2** with CO were studied. Figure 3A shows the FTIR spectrum of a solution of **1** after it was saturated by bubbling with CO for ten minutes. In addition to the 1918 cm^{-1} signal of the parent complex, two new CO stretching bands are observed at 1996 and 2020 cm^{-1} indicating formation of an $Fe(CO)_2S_2P_2$ complex, **1-CO**. The presence of two new bands indicates that the CO ligands are in a *cis* orientation. The ^{31}P NMR spectrum obtained under the same conditions also includes both the 66.32 ppm resonance of the starting material and a new signal at 62.59 ppm, providing additional evidence for formation of **1-CO**. Following removal of CO from the solution by purging with nitrogen, the signals associated with **1-CO** were no longer present. This demonstrates that binding of external CO to **1** is a reversible process. The analogous reaction for **2** was also observed *via*

identification of new CO stretches at 1995 and 2021 cm^{-1} (Figure 3B). The complex **2-CO** also reverted reversibly to **2** upon removal of the CO. We note, however, that formation of **2-CO** was less complete than formation of **1-CO**. The complex **2-CO** was not produced in quantities sufficient to be detected by ^{31}P NMR. Furthermore, the ratios of the intensities of the CO stretching bands in the IR spectrum also suggest that the majority of **2** remains unreacted. The difference in reactivities of the two complexes may be attributable to the geometries about the iron centers. Formation of a *cis* dicarbonyl from **2** will require a substantial distortion with one of the extant ligands moving to a position *trans* to a carbonyl. However, such a large rearrangment is not required for the reaction of **1**.

Addition of the strong acid $HBF_4.OEt_2$ facilitated a quantitative reaction between **1** and CO. The newly formed complex, **[1(H)-CO]**$^+$, is red in solution and has characteristic CO stretching vibrations at 2089 and 2043 cm^{-1} (Figure 3C). Complex **1** could be reversibly regenerated from **[1(H)-CO]**$^+$ by purging the solution with nitrogen and addition of triethylamine. An analogous reaction of **2** was not observed under the same conditions. The relative intensities of and energy gap between the two signals associated with CO stretching in the IR spectrum of **[1(H)-CO]**$^+$ are reminiscent of the well-characterized *cis,cis,cis*-$Fe(CO)_2(dppe)(SPh)_2$ which has analogous peaks at 2017 and 1970 cm^{-1}.[41] Most notable is that the stretching frequencies of **[1(H)-CO]**$^+$ are 73 cm^{-1} higher in energy compared to this reference compound. This shift can be explained by the requirement for acid for this reaction. Since bdt complexes of transition metals can have mixed metal-ligand character frontier orbitals (*vide infra*), the complex is likely protonated at one of the sulfurs, resulting in a substantially weaker ligand and

increasing the electrophilicity of the metal center.[42-44] The result is less back-bonding into the π* LUMO of the CO and a stronger CO bond reflected in a higher energy stretch. Such enhanced electrophilicity of a d^6 metal ion on ligand protonation is not unprecedented.[23, 45] Hence we postulate that the protonated dicarbonyl species is *cis,cis,cis*-$[Fe(CO)_2(\kappa^2\text{-dppf})(bdt\text{-}H)]^+$.

Electrochemistry and catalysis. The redox transitions of the two complexes were probed by cyclic voltammetry. Electrochemical analysis of **1** and **2** in 0.1 M $[NBu_4][PF_6]$/THF was performed under an argon atmosphere. As shown in Figure 5, cyclic voltammograms of **1** show a reversible reduction at $E_{1/2}$= -1.65 V (i_p^a/i_p^c = 0.99, ΔE_p= 0.144 V) and two reversible oxidations at $E_{1/2}$= +0.13 V (i_p^c/i_p^a = 0.90, ΔE_p= 0.140 V) and +0.44 V (i_p^c/i_p^a = 0.98, ΔE_p = 0.137 V) *vs.* $Fc^{+/0}$ (Fc = ferrocene). Controlled potential coulometry shows that the reduction at -1.65 V is a one-electron process (Figure S1), and it likely corresponds to the $Fe^{II/I}$ couple of the pentacoordinate Fe center. We note that a second, smaller reduction peak can be observed on close inspection which may indicate a second, more complicated, reduction process also occurs to a limited extent. The oxidations at +0.13 and +0.44 V can be assigned to the $Fe^{III/II}$ couples for the Fe center in dppf and the pentacoordinate Fe center. The oxidation wave at +0.13 V is likely associated with the oxidation of the Fe^{II} center in dppf since quasi-reversible oxidation of free dppf occurs at $E_{1/2}$= 0.183 V in 1,2-dichloroethane.[46, 47] On the other hand, cyclic voltammograms of **2** reveal that it undergoes a reversible, one-electron reduction at $E_{1/2}$ = -1.86 V (i_p^a/i_p^c = 0.96, ΔE_p = 0.164 V) and an irreversible one-electron oxidation at $E_{1/2}$= +0.32 V. By analogy to **1**, the reduction and oxidation waves are likely to be $Fe^{II/I}$ and $Fe^{III/II}$ couples, respectively. Notably, reduction of the pentacoordinate Fe^{II}

center in **2** occurs at more negative potential than **1**. More interestingly, in contrast to the two reversible $Fe^{III/II}$ couples in **1**, the $Fe^{III/II}$ couple in **2** is irreversible, indicating coordination of dppf leads to improved stability of oxidized complex in $Fe^{III}Fe^{II}$ and $Fe^{III}Fe^{III}$ states. In the case of **2**, oxidation of the pentacoordinate Fe^{II} center might be associated with a geometry change, subsequent reaction with solvent molecules, or ligand dissociation.

The electrocatalytic proton reduction activities of **1** and **2** were investigated in THF in the presence of acetic acid ($pK_{a(THF)}$ = 24.42)[48] and *p*-toluenesulfonic acid (*p*-TsOH). As shown in Figure 6, sequential addition of acetic acid from 0.2 M to 1.4 M renders the reduction wave for the $Fe^{II/I}$ couple irreversible and leads to an increase in current. This is characteristic of electrocatalytic proton reduction since direct proton reduction from acetic acid at the glassy carbon electrode is negligible in this potential range (see Supporting Information, Figure S2).[49, 50] Production of hydrogen gas was verified by GC analysis and Faradaic efficiency of hydrogen production was determined to be 93% for **1** and 96% for **2**. The overpotentials for proton reduction by the two complexes, determined using the method reported by Artero and co-workers, were relatively small, only 0.17–0.2 V and 0.38–0.43 V for **1** and **2**, respectively (Table S2).[51] The half-wave potentials for the catalytic current, used for the overpotential calculation, were determined as the potential corresponding to the maximum value of (di/dE), *i.e.* the first derivative of the current data from the cyclic voltammograms. For comparison, a mononuclear iron complex $\{\kappa^2\text{-}(Ph_2PCH_2N(X)CH_2PPh_2)\}Fe(CO)(\kappa^2\text{-bdt})$ (X = 1,1-diethoxy-ethyl) similar to **2** was reported to reduce protons from acetic acid in acetonitrile with overpotential in the range 0.23–0.27 V.[27] The kinetics of proton

reduction were evaluated by considering the effect of catalyst concentration and acid concentration on observed activity (see Figures S3 and S4). Figure S3 shows that catalytic peak current, i_{cat}, depends linearly on catalyst concentration, [cat], for both **1** and **2**. This demonstrates a first-order dependence of the catalytic current on the concentration of the catalyst at fixed acid concentrations as described by eq. 1 in which *n* is the number of electrons involved in the catalytic reaction, *A* is the area of the electrode, *D* is the diffusion coefficient of the catalyst, *k* is the rate constant and *x* is the order of the reaction with respect to acid.[52] Figure S4 shows that the ratio of catalytic current to reductive peak current measured in the absence of acid, i_{cat}/i_p, is also linear with respect to acid concentration for catalyst concentrations in the range 0.74–1.13 mM for **1** and 0.47–1.35 mM for **2**. This indicates the reaction is second-order with respect to acid concentration as described by eq. 2, for a scan rate υ of 0.1 V s^{-1}. At the highest acid concentration investigated (1.6 M), a value of i_{cat}/i_p of 35 was obtained for **2** (0.6 mM), corresponding to a turnover frequency of 241 s^{-1}. A much slower rate was observed for **1** (0.74 mM) with a turnover frequency of 10 s^{-1} in 1.8 M acetic acid.

$$i_{cat} = nFA[cat]\sqrt{D(k[acid]^x)} \qquad (1)$$

$$i_{cat}/i_p = \left(\frac{n}{0.4463}\right)\sqrt{RT(k[acid]^x)/F\nu} \qquad (2)$$

The electrocatalytic activities of the two complexes were also studied in the presence of the stronger acid, *p*-TsOH (p-toluenesulfonic acid monohydrate). Irreversible catalytic waves corresponding to the reduction of protons are observed at the potentials of the **1**/**1**$^-$ and **2**/**2**$^-$ couples (Figure 7). Figure S9 shows voltammograms demonstrating that direct reduction by the electrode surface requires substantially higher overpotentials. The catalytic peak current is largely independent of catalyst concentration (panel B of Figure

S5) for **1** over the investigated range (0.28–0.83 mM) and increases linearly with increasing concentration of *p*-TsOH (panel A of Figure S5). A similar result has been reported for the mononuclear iron complex analogous to **2** incorporating a different NP_2 ligand, N,N-bis{(diphenylphosphino)methyl}-2,2-diethoxyethanamine.[27] Interestingly, for both **1** and **2**, at low concentration of *p*-TsOH (1-2 eq. of the catalyst), a new reduction wave at 150 mV less negative potential is observed together with the original $Fe^{II/I}$ couple which grows with increasing acid concentration (Figure S6). However, at higher acid concentration (more than 2 eq.), the two peaks merge to produce a single catalytic wave. The observation that this new peak emerges for both complex **1** and **2** excludes the possibility that it is associated with protonation at the amine group of the NP_2 ligand in **2**. Association between either the sulfurs or the aromatic ring of the bdt ligand and the proton/acid is, however, a distant possibility.

Computational Studies. To complement the experimental results, density functional theory (DFT) calculations were carried out on **1**, **2**, $\mathbf{1(H)^+}$, $\mathbf{2(H)^+}$, $\mathbf{[1(H)\text{-}CO]^+}$, and $\mathbf{[2(H)\text{-}CO]^+}$. Calculations were performed using the B3LYP hybrid functional and the 6-31G* basis set, and the DFT-optimized structures, which agree well with the corresponding crystal structures for complexes **1** and **2**, were confirmed as energy minima. A detailed comparison of calculated and experimental metric parameters can be found in Table S3. The calculated frontier molecular orbitals for the complexes **1**, **2**, $\mathbf{1(H)^+}$, and $\mathbf{2(H)^+}$ are shown in Figure 8. Similarly, Figure 9 shows the frontier molecular orbitals for $\mathbf{[1(H)\text{-}CO]^+}$, and $\mathbf{[2(H)\text{-}CO]^+}$. Complexes **1** and **2** both have HOMOs that are delocalized over the Fe and much of the bdt ligand. In particular, the HOMOs are a bonding combination of iron d orbitals and sulfur p(π) orbital(s), and an antibonding

combination of sulfur and the adjacent carbon atoms, implying strong electron delocalization over the iron and the bdt ligand (Supplementary Information, Table S5).[53-55] It is worth noting, however, that from the perspective of the frontier molecular orbitals, the Fe-S interactions are not equivalent for the two complexes. The HOMO of **1** includes interactions only between the Fe and the axial sulfur, likely a result of the unusual geometry. On the other hand, the HOMO of **2** includes substantial contributions from both sulfurs of the bdt ligand. Furthermore, the HOMOs of **1** and **2** bear considerable resemblance to the HOMO of the free bdt^{2-} ligand or the SOMO of the free ligand in the π-radical anion form ($bdt^{-\bullet}$).[56, 57] From the molecular orbital approach, the metal dithiolate interaction in both complexes can best be described as resulting from transfer of electron density from the HOMO of the bdt^{2-} ligand to empty Fe *d* orbitals. On the other hand, the orbital density profiles shown in Figure 8 and the percentage orbital contribution given in Table S5 indicate that the LUMOs are dominated primarily by contributions from the Fe *d* orbitals with the sulfur and phosphorus atoms playing a minor role. There is almost no contribution from the rest of the ring structure to the LUMOs. This suggests that reduction of the complexes results in substantial accumulation of charge localized at the metal center yielding a highly basic iron site for interaction with protons. Furthermore, the significant iron character of the LUMOs (51% and 43% for **1** and **2**, respectively) is consistent with the abilities of these complexes to reversibly bind CO.

Additionally, Mulliken charge decomposition analysis was used to quantify charge transfer between various fragments within each complex. The Mulliken charge decomposition analysis values (Table S7) are consistent with the frontier molecular

orbital bonding description above. The ferrocenyl Fe of the phosphine ligand of **1** has a charge in the narrow range of +0.46 to +0.48 throughout all complexes in which it is present, i.e. it serves as an internal standard for the value expected for Fe(II) using this computational method. This value is very similar to the +0.4 determined in a recent Löwdin population analysis.[58] The catalytically active Fe always carries a less positive charge indicating a net transfer of charge from the ligands to the metal to achieve lower than 2+ oxidation state.

To correlate the observed trends in the reactivity of the two complexes with CO in the presence of acid, DFT calculations were also undertaken for the protonated complexes, $\mathbf{1(H)}^+$ and $\mathbf{2(H)}^+$, assuming compositional integrity following protonation. For complex **1**, protonation is most likely to occur at either the Fe center or the thiolate sulfur with the highest contribution to the HOMO.[59] The possibilities for **2** are more numerous since both the sulfurs contribute to the HOMO and it features an amine group in the NP_2 ligand that could also serve as a protonation site. Calculations for $\mathbf{1(H)}^+$ with the proton localized on the Fe indicate that it is 13 kcal/mol higher in energy than a $\mathbf{1(H)}^+$ complex with a protonated thiolate. Likewise, in the case of **2**, an N-protonated species is 6.4 kcal/mol higher in energy than the S-protonated species. Therefore, the rest of the computational studies were carried out assuming that protonation occurs exclusively at the thiolate sulfur. The geometry optimized structure of $\mathbf{1(H)}^+$ shows that protonation results in only minor changes about the Fe center; in particular, the τ value of $\mathbf{1(H)}^+$, 0.65, is not significantly different from that of **1**, 0.72 (Supplementary Information, Table S3). In contrast, upon protonation, **2** undergoes considerable distortion from its nearly square pyramidal geometry (τ = 0.09) to a hybrid of square pyramidal and trigonal bipyramidal

geometries (τ = 0.42). Furthermore, electron density profiles of the HOMO and LUMO of **1(H)**$^+$ and **2(H)**$^+$ reveal stark differences that are important for understanding their different reactivities towards CO. The HOMO of **1(H)**$^+$ is localized entirely on the ferrocene moiety, while the HOMO of **2(H)**$^+$ is delocalized over the entirety of the bdt ligand with minimal contribution from the Fe atom. The bonding pattern in the bdt ligand and the orbital contributions in the HOMO suggest that in **2(H)**$^+$, the bdt ligand is partially oxidized resulting in a charge on the Fe center less than +2. The Mulliken charge decomposition analysis also suggests that one of the thiolate sulfurs is noticeably less negative in **2(H)**$^+$ than **2,** and the aromatic ring also carries less negative charge. On the other hand, the orbital analysis suggests that addition of a proton to **1** disrupts the electron delocalization between the bdt ligand and the Fe center, reinstating the aromaticity of the C_6H_4-ring of the protonated bdt ligand. Therefore, **1(H)**$^+$ is expected to behave more like a typical coordinatively unsaturated Fe^{II}, d^6 complex, i.e. to bind exogenous ligand. This difference in the electronic structures of **1(H)**$^+$ and **2(H)**$^+$ is likely responsible for the fact that protonation induced CO uptake is observed only for **1**.

Simple frontier orbital concepts also suggest that the interaction of CO will be stronger with **1(H)**$^+$ than with **2(H)**$^+$. The LUMO of **1(H)**$^+$ is about 0.1 eV lower in energy than that of **2(H)**$^+$. Since the HOMO of CO has an energy of ~-10.1 eV, it is expected to interact more strongly with **1(H)**$^+$. Addition of a CO molecule to either **1(H)**$^+$ or **2(H)**$^+$ requires a change to octahedral geometry to accommodate the new ligand resulting in sp^3d^2 hybridization involving the d_{z^2} and $d_{x^2-y^2}$ orbitals. Thus, the enhanced contributions of d_{z^2} and $d_{x^2-y^2}$ orbitals to the LUMO of **1(H)**$^+$ clearly indicate that addition of CO to **1(H)**$^+$ would be more facile than to **2(H)**$^+$ (Table S5). Finally, it is worth noting

that for related pentacoordinate complexes Ott and coworkers have predicted that complexes in square pyramidal geometry should be more reactive than trigonal bipyramidal especially in the presence of bulky ligands.[29] Our experimental results suggest the opposite for these complexes, but it is important to remember that geometries observed in the solid state may be different from those found in solution.

Calculations of the CO bound protonated complexes, **[1(H)-CO]**$^+$ and **[2(H)-CO]**$^+$, show that *trans* attachment of the second CO molecule is more favorable than *cis* attachment by 1.4 and 1.0 kcal/mol, respectively. However, in all reactions, the *cis* complex was detected via FTIR spectroscopy. This may indicate that the reaction is under kinetic control under these experimental conditions. It is worth noting that in all cases, i.e. both *cis* and *trans* attachment, charge decomposition analysis suggests that carbonylation results in a significant increase in electron density at Fe1. In large part, this electron density comes at the expense of that in the CO ligands (Table S7). The structural data also suggests a lengthening of the Fe-C bonds and a shortening of the CO bonds accompanies attachment of the second CO (Table S3). These computational results are consistent with the FTIR experiments, demonstrating a shift of the CO stretches to higher energy for complexes **[1(H)-CO]**$^+$ and **[2(H)-CO]**$^+$.

Conclusion

In summary, we have synthesized two pentacoordinate $Fe^{II}(CO)P_2S_2$ complexes using benzene-1,2-dithiol and two different chelating bis-phosphine ligands: NP_2 and dppf. Although the electronic properties of both phosphines are comparable and the resulting complexes might be expected to be similar, the differing geometrical constraints

of the two phosphines result in complexes with dramatically different reactivity. In the solid state, in contrast to the SP complex formed with NP_2, the wider bite-angle of dppf results in formation of a TBP complex. These geometric differences lead to significant changes in both the electronic and the chemical properties of the complexes including reactivity towards CO, reduction potentials, electrocatalytic activity, and energies of charge-transfer bands. These observations may prove important both in understanding the reactivity of natural enzymes and functional small molecule mimics *and* in constructing more effective functional catalysts.

Two recent examples emphasize the importance of geometric constraints on production of efficient proton reduction catalysts. First, assembly of an active hydrogenase by incorporation of an inactive, inorganic model into the active site of an apo-[FeFe]-hydrogenase highlights the importance of geometric constraints from a protein in forcing unexpected reactivity at metallocenters.[60] Second, the $[Ni(P^{Ph}_2N^{Ph})_2]^{2+}$ catalyst of the DuBois group is approximately two orders of magnitude faster than the closely related $[Ni(P^{Ph}_2N^{C_6H_4X_2})_2]^{2+}$ cousins; this is likely due in part to the planarity at the nickel center imposed by the different geometric requirements of the ligands influencing the hydricity of the Ni-H bond.[52] Complexes **1** and **2** offer another example in which the metal geometry imposed by the steric constraints of the phosphine ligand has a dramatic impact on resulting chemical properties. Both computational studies and single crystal X-ray structures suggest that the bdt ligand is partially oxidized in both complexes and, as a result of the extensive π-overlap between the metal and the ligand, the overall charge on the iron is less than +2. However, the π-interaction between the iron and the bdt in **1** is more flexible, allowing the complex to behave as might be expected for an unsaturated

Fe(II) complex and undergo proton induced CO uptake to produce an 18-electron complex. The same unusual electronic environment also allows **1** to reduce protons with less overpotential than **2**, albeit at considerably reduced rates. Unfortunately, this classic trade-off between rate and overpotential continues to be a problem for synthetic proton reduction catalysts. Nonetheless, we anticipate that this combination of unusual ligands geometry together with redox active ligands may prove fruitful in developing reversible catalysts for hydrogen production and oxidation that function with minimal overpotentials.

Experimental Section

All reactions were carried out under an atmosphere of nitrogen using standard Schlenk and vacuum-line techniques unless otherwise noted. Anhydrous dichloromethane and methanol were purchased from Sigma-Aldrich and deuterated solvents from Cambridge Isotope Laboratories. Tetrahydrofuran was dried by distilling overnight over sodium and benzophenone. All starting materials were obtained commercially and used without further purification. ^{1}H, ^{13}C and ^{31}P NMR spectra were recorded at room temperature on a Varian Liquid-State NMR spectrometer (400 or 500 MHz for ^{1}H). NMR chemical shifts are quoted in ppm; spectra were referenced to tetramethylsilane for ^{1}H and ^{13}C NMR. The ^{31}P NMR spectra were referenced to external phosphoric acid at 0 ppm. FTIR spectra were recorded on a Bruker vertex 70 spectrophotometer using a stainless steel sealed liquid spectrophotometer cell with CaF_2 windows. UV-vis measurements were performed on a Hewlett-Packard 8453 spectrophotometer using quartz cuvettes with a 1 cm pathlength.

Synthesis of methyl 2-(bis(diphenylphosphinomethyl)amino)acetate, NP_2. To an anaerobic solution of formaldehyde (37 wt.% in water; 1 mL, 12.3 mmol) in absolute ethanol (10 mL), diphenylphosphine (1.9 mL, 10.9 mmol) was added dropwise under argon. The reaction mixture was stirred at room temperature for 30 min followed by addition of glycine methyl ester hydrochloride (0.7 g, 5.6 mmol) in 40% aqueous ethanol (5 mL). The cloudy reaction mixture became clear on stirring for 2 h. Volatile materials were removed under reduced pressure to afford a colorless oily residue. The crude product was purified *via* column chromatography on silica with hexane/ethyl acetate/triethylamine (66:33:1) as eluent to afford NP_2 as a colorless oil. Yield: 2.4 g (85%). R_f = 0.85 (1:1 hexane/ethyl acetate, 1% NEt_3). ^1H NMR (400 MHz, $CDCl_3$): δ = 7.38 (m, 8H), 7.26 (m, 12H), 3.81 (s, 2H), 3.7 (d, 4H), 3.61 (s, 3H). $^{13}C\{^1H\}$ NMR (100 MHz, $CDCl_3$): δ = 171.21, 137.58, 137.46, 133.09, 132.90, 128.57, 128.37, 128.34, 128.30, 58.02, 55.65, 51.28. $^{13}P\{^1H\}$ NMR (161.8 MHz, $CDCl_3$): δ = -27.19.

Synthesis of (dppf)Fe(CO)(bdt), 1. To an anaerobic solution of anhydrous $FeCl_2$ (60.3 mg, 0.48 mmol) in anhydrous methanol (8 mL), 1,1'-bis(diphenylphosphino)ferrocene (280 mg, 0.5 mmol) in THF (4 mL) was added dropwise under a CO atmosphere. After stirring the reaction mixture for 30 min at room temperature, a solution of benzene-1,2-dithiol (0.07 mL, 0.6 mmol) and triethylamine (0.17 mL, 1.2 mmol) in methanol (3 mL) was added dropwise. The reaction turned to violet and then to dark brown. After stirring for 1 h at room temperature, the solvent was removed under reduced pressure, and the residue was purified *via* column chromatography on silica with hexane/dichloromethane (1:2) as eluent. The product was obtained as dark brown powder. Yield: 244 mg (65%). R_f = 0.4 (1:1 hexane/CH_2Cl_2). ^1H

NMR (400 MHz, CD_2Cl_2): δ = 8.04 (dd, *J* = 6.0, 3.2 Hz, 2H), 7.59 (m, 4H), 7.41-7.36 (m, 8H), 7.18-7.10 (m, 10H), 4.89 (s, 2H), 4.48 (s, 2H) 4.24 (s, 2H), 4.12 (s, 2H). $^{13}C\{^1H\}$ NMR(100 MHz, CD_2Cl_2): δ = 134.98, 132.71, 130.39, 129.50, 129.32, 127.76, 127.41, 121.38, 76.96, 74.92, 74.79, 72.60, 71.40. $^{31}P\{^1H\}$ NMR (161.8 MHz, CD_2Cl_2): δ = 66.32. IR (CH_2Cl_2, cm^{-1}): ν(CO) 1918. APCI mass spectrum (positive mode): 751.0198 $[(M\text{-}CO+H)^+]$.

Synthesis of $(NP_2)Fe(CO)(bdt)$, 2. To an anaerobic solution of anhydrous $FeCl_2$ (75 mg, 0.6 mmol) and NP_2 ligand (264 mg, 0.56 mmol) in anhydrous methanol (11 mL) under a CO atmosphere, benzene-1,2-dithiol (0.07 mL, 0.6 mmol) and triethylamine (0.17 mL, 1.2 mmol) were added. The color of the solution turned black. After stirring at room temperature for 2 h, the solvent was removed under reduced pressure and the residue was purified *via* column chromatography on silica with hexane/ethyl acetate (4:1) as eluent. The desired compound was obtained as a green solid. Yield: 240 mg (60%). R_f = 0.3 (3:1 hexane/ethyl acetate). ^1H NMR (400 MHz, CD_2Cl_2): δ = 7.99 (dd, *J* = 6, 3.2 Hz 2H), 7.64 (m, 4H), 7.50 (m, 6H), 7.15 (m, 6H), 7.09 (dd, *J* = 6, 3.2 Hz, 2H), 6.96 (t, *J* = 7.6 Hz, 4H), 4.05-3.97 (m, 2H), 3.86-3.80 (m, 2H), 3.70 (s, 3H), 3.59 (s, 2H). ^{13}C NMR (100 MHz, CD_2Cl_2): δ = 133.68 (t), 132.74 (t), 130.46 (s), 129.83 (s), 129.05 (s), 128.42 (t), 127.82 (t), 121.34 (s), 62.00 (t), 56.73 (s) 56.57 (s), 51.64 (s). ^{31}P NMR (161.8 MHz): δ = 50.21. IR (CH_2Cl_2, cm^{-1}): ν(CO) 1915. APCI mass spectrum (positive mode): m/z = 710.0799 $[(M+H)^+]$, 682.0787 $[(M\text{-}CO+H)^+]$.

Reaction of 1 with CO in the presence of $HBF_4.OEt_2$. A solution of **1** (3.2 mg, 4.1 μmol) in CH_2Cl_2 (2 mL) was saturated with CO and $HBF_4{\bullet}OEt_2$ (0.2 mL 0.074 M solution in CH_2Cl_2, 14.3 μmol, 3.6 equivalent) was added dropwise to the reaction

mixture. After stirring for 10 min at room temperature, the color of the solution changed from dark brown to red. Formation of the CO adduct $[\mathbf{1(H)\text{-}CO}]^+$ was indicated by IR and ^{31}P NMR. Addition of triethylamine (0.04 mL, 28.6 μmol) to the reaction mixture followed by purging with N_2 led to release of CO and quantitative regeneration of **1**. IR (CH_2Cl_2): ν(CO) 2089, 2043. ^{31}P $\{^1H\}$ NMR (161.8 MHz, CD_2Cl_2): δ = 4.92.

X-ray crystallography. A representative crystal of each compound was individually mounted on the end of a thin glass fiber using Apiezon type N grease and optically centered. Cell parameter measurements and single-crystal diffraction data collection were performed at low temperature (123 K) with a Bruker Smart APEX diffractometer. Graphite monochromated Mo Kα radiation (λ = 0.71073 Å) in the ω–φ scanning mode was used for the measurements. The structure was solved by direct methods and refined by fullmatrix least-squares on F^2. The following is the list of the programs used: data collection, Bruker Instrument Service v2010.9.0.0; cell refinement and data reduction, SAINT V7.68A; structure solution and refinement, SHELXS-97; molecular graphics, XShell v6.3.1; preparation of material for publication, Bruker APEX2 v2010.9-1.30. Details of crystal data and parameters for data collection and refinement are listed in Table S1.

Electrochemistry. Electrochemical experiments were carried out using either a CHI 1200A electrochemical analyzer or a PG-STAT 128N Autolab electrochemical analyzer. A conventional three-electrode cell was used for recording cyclic voltammograms. The working electrode was a 3 mm diameter glassy carbon disk polished with 1 mm and 0.3 mm deagglomerated alpha alumina, successively, and sonicated for 15 min in ultrapure water prior to use. The supporting electrolyte was

$[NBu_4][PF_6]$ (0.1 M in THF). The Ag/Ag^+ reference electrode was prepared by immersing a silver wire anodized with AgCl in an THF solution of 0.1 M $[NBu_4][PF_6]$. A platinum wire was used as counter electrode. Deaeration of the solutions was performed by bubbling argon through the solution for 15 min after which an atmosphere of Ar was maintained during the course of electrochemical measurements. All potentials are reported relative to the ferrocene couple (Fc^+/Fc) as reference. Concentrations of the complexes were determined spectrophotometrically based on the following extinction coefficients: ε(467 nm) = 4433 M^{-1} cm^{-1} and ε(437 nm) = 4537 $M^{-1}cm^{-1}$ for **1** and **2**, respectively.

Bulk electrolysis experiments were undertaken in a sealed BASi bulk electrolysis cell under an Ar atmosphere. The working electrode was a reticulated vitreous carbon electrode (cylinder of 40 mm diameter, 50 mm height, and 5 mm depth). A non-aqueous (THF) Ag/AgCl reference electrode was placed in a separate compartment and connected via a fine porosity glass frit. A platinum wire was used as counter electrode. The electrochemical cell was sealed following 15 minutes of deaeration with argon. For determination of the quantity of hyrogen produced, samples were removed from the headspace of the cell via a Hamilton locking gas-tight syringe, and an equal volume of argon was concomitantly added. Following calibration with H_2 samples of known concentration, a Varian CP-3800 gas chromatograph (thermal conductivity detector, Alltech Porapak Q 80/100 column, Ar as carrier gas) was used to separate the headspace samples and quantify the amount of hydrogen present.

Computational Details. Density functional theory (DFT) calculations were carried out using the Becke gradient-corrected exchange functional and Lee−Yang−Parr

correlation functional with three parameters (B3LYP) and the 6-31G* basis set.[59, 61-69] This level of theory has been found to yield reliable geometries and vibrational frequencies for a number of first-row transition metal systems.[70-74] Nonetheless, in light of recent studies indicating the improved performance of the BP86 and TPSS functionals in describing transition metal containing systems, the geometries and energies of **2** were also calculated using these functionals and the larger TZVPP basis sets.[75-77] These results are shown in Table S4 which indicate that the B3LYP/6-31G* level of theory is reliable for the systems investigated in this study. The "overlap population" parameter listed in Tables S5 and S6 is a measure of the nature of the interaction between the orbitals involved. Thus, a positive overlap population represents a bonding interaction, a negative overlap population corresponds to an anti-bonding interaction, and a zero overlap population indicates no bonding between the fragments.

Supporting Information Available: Additional electrochemical data and ^{1}H NMR spectra. Selected X-ray crystal structural data. Description of the method for determining electrocatalytic overpotential. Summary of structural data, orbital contributions and overlap populations calculated via DFT and, where appropriate, compared to X-ray analysis. Benchmark calculations. Mulliken charge decomposition analysis values. This material is available free of charge via the Internet at http://pubs.acs.org.

Acknowledgements: This research was supported through the Center for Bio-Inspired Solar Fuel Production, an Energy Frontier Research Center funded by the U.S.

Department of Energy, Office of Science, Office of Basic Energy Sciences under Award Number DE-SC0001016.

References

1. Armstrong, F. A., *Science* **2013,** *339*, 658-659.

2. Vignais, P. M.; Billoud, B., *Chem. Rev.* **2007,** *107*, 4206-4272.

3. Tard, C.; Pickett, C. J., *Chem. Rev.* **2009,** *109*, 2245-2274.

4. Volbeda, A.; Charon, M.-H.; Piras, C.; Hatchikian, E. C.; Frey, M.; Fontecilla-Camps, J. C., *Nature* **1995,** *373*, 580-587.

5. Peters, J. W.; Lanzilotta, W. N.; Lemon, B. J.; Seefeldt, L. C., *Science* **1998,** *282*, 1853-1858.

6. Nicolet, Y.; Piras, C.; Legrand, P.; Hatchikian, C. E.; Fontecilla-Camps, J. C., *Struct. Fold. Des.* **1999,** *7*, 13-23.

7. Happe, R. P.; Roseboom, W.; Pierik, A. J.; Albracht, S. P. J.; Bagley, K. A., *Nature* **1997,** *385*, 126-126.

8. Evans, D. J.; Pickett, C. J., *Chem. Soc. Rev.* **2003,** *32*, 268-275.

9. Jones, A. K.; Sillery, E.; Albracht, S. P. J.; Armstrong, F. A., *Chem. Commun.* **2002**, 866-867.

10. Madden, C.; Vaughn, M. D.; Diez-Perez, I.; Brown, K. A.; King, P. W.; Gust, D.; Moore, A. L.; Moore, T. A., *J. Am. Chem. Soc.* **2012,** *134*, 1577-1582.

11. Felton, G. A. N.; Mebi, C. A.; Petro, B. J.; Vannucci, A. K.; Evans, D. H.; Glass, R. S.; Lichtenberger, D. L., *J. Organomet. Chem.* **2009,** *694*, 2681-2699.

12. Gloaguen, F.; Rauchfuss, T. B., *Chem. Soc. Rev.* **2009,** *38*, 100-108.

13. Stoian, S. A.; Hsieh, C.-H.; Singleton, M. L.; Casuras, A. F.; Darensbourg, M. Y.; McNeely, K.; Sweely, K.; Popescu, C. V., *J. Biol. Inorg. Chem.* **2013,** *18*, 609-622.

14. Wang, W.; Rauchfuss, T. B.; Moore, C. E.; Rheingold, A. L.; De Gioia, L.; Zampella, G., *Chem-Eur. J.* **2013,** *19*, 15476-15479.

15. Hsieh, C. H.; Erdem, O. F.; Harman, S. D.; Singleton, M. L.; Reijerse, E.; Lubitz, W.; Popescu, C. V.; Reibenspies, J. H.; Brothers, S. M.; Hall, M. B.; Darensbourg, M. Y., *J. Am. Chem. Soc.* **2012,** *134*, 13089-13102.

16. Darensbourg, M. Y.; Lyon, E. J.; Zhao, X.; Georgakaki, I. P., *Proc. Natl. Acad. Sci. USA* **2003,** *100*, 3683-3688.

17. Siegbahn, P. E. M.; Tye, J. W.; Hall, M. B., *Chem. Rev.* **2007,** *107*, 4414-4435.

18. Armstrong, F. A., *Curr. Opin. Chem. Biol.* **2004,** *8*, 133-140.

19. Darensbourg, D. J.; Reibenspies, J. H.; Lai, C.-H.; Lee, W.-Z.; Darensbourg, M. Y., *J. Am. Chem. Soc.* **1997,** *119*, 7903-7904.

20. Hsu, H.-F.; Koch, S. A.; Popescu, C. V.; Münck, E., *J. Am. Chem. Soc.* **1997,** *119*, 8371-8372.

21. Lai, C.-H.; Lee, W.-Z.; Miller, M. L.; Reibenspies, J. H.; Darensbourg, D. J.; Darensbourg, M. Y., *J. Am. Chem. Soc.* **1998,** *120*, 10103-10114.

22. Liaw, W.-F.; Lee, N.-H.; Chen, C.-H.; Lee, C.-M.; Lee, G.-H.; Peng, S.-M., *J. Am. Chem. Soc.* **2000,** *122*, 488-494.

23. Liu, T.; Li, B.; Popescu, C. V.; Bilko, A.; Pérez, L. M.; Hall, M. B.; Darensbourg, M. Y., *Chem. Eur. J.* **2010,** *16*, 3083-3089.

24. Shima, S.; Pilak, O.; Vogt, S.; Schick, M.; Stagni, M. S.; Meyer-Klaucke, W.; Warkentin, E.; Thauer, R. K.; Ermler, U., *Science* **2008,** *321*, 572-575.

25. Sellmann, D.; Kleine-Kleffmann, U.; Zapf, L.; Huttner, G.; Zsolnai, L., *J. Organomet. Chem.* **1984,** *263*, 321-331.

26. Rauchfuss, T. B.; Contakes, S. M.; Hsu, S. C. N.; Reynolds, M. A.; Wilson, S. R., *J. Am. Chem. Soc.* **2001,** *123*, 6933-6934.

27. Beyler, M.; Ezzaher, S.; Karnahl, M.; Santoni, M.-P.; Lomoth, R.; Ott, S., *Chem. Commun.* **2011,** *47*, 11662-11664.

28. Gardner, J. M.; Beyler, M.; Karnahl, M.; Tschierlei, S.; Ott, S.; Hammarstrom, L., *J. Am. Chem. Soc.* **2012,** *134*, 19322-19325.

29. Orthaber, A.; Karnahl, M.; Tschierlei, S.; Streich, D.; Stein, M.; Ott, S., *Dalton Trans.* **2014,** *43*, 4537-4549.

30. Bandoli, G.; Dolmella, A., *Coord. Chem. Rev.* **2000,** *209*, 161-196.

31. Bandoli, G.; Trovo, G.; Dolmella, A.; Longato, B., *Inorg. Chem.* **1992,** *31*, 45-51.

32. Butler, I. R.; Cullen, W. R.; Kim, T. J.; Rettig, S. J.; Trotter, J., *Organometallics* **1985,** *4*, 972-980.

33. Longato, B.; Pilloni, G.; Valle, G.; Corain, B., *Inorg. Chem.* **1988,** *27*, 956-958.

34. Durran, S. E.; Elsegood, M. R. J.; Hawkins, N.; Smith, M. B.; Talib, S., *Tetrahedron Lett.* **2003,** *44*, 5255-5257.

35. Addison, A. W.; Rao, T. N.; Reedijk, J.; van Rijn, J.; Verschoor, G. C., *J. Chem. Soc., Dalton Trans.* **1984**, 1349-1356.

36. Nguyen, D. H.; Hsu, H.-F.; Millar, M.; Koch, S. A.; Achim, C.; Bominaar, E. L.; Munck, E., *J. Am. Chem. Soc.* **1996,** *118*, 8963-8964.

37. Hsu, H.-F.; Koch, S. A.; Popescu, C. V.; Münck, E., *J. Am. Chem. Soc.* **1997,** *119*, 8371-8372.

38. Ray, K.; Begum, A.; Weyhermuller, T.; Piligkos, S.; van Slageren, J.; Neese, F.; Wieghardt, K., *J. Am. Chem. Soc.* **2005,** *127*, 4403-4415.

39. Ray, K.; Bill, E.; Weyhermuller, T.; Wieghardt, K., *J. Am. Chem. Soc.* **2005,** *127*, 5641-5654.

40. Ray, K.; Weyhermuller, T.; Goossens, A.; Craje, M. W. J.; Wieghardt, K., *Inorg. Chem.* **2003,** *42*, 4082-4087.

41. Takacs, J.; Marko, L.; Parkanyi, L., *J. Organomet. Chem.* **1989,** *361*, 109-116.

42. Waters, T.; Wang, X.-B.; Woo, H.-K.; Wang, L.-S., *Inorg. Chem.* **2006,** *45*, 5841-5851.

43. Benedito, F. L.; Petrenko, T.; Bill, E.; Weyhermuller, T.; Wieghardt, K., *Inorg. Chem.* **2009,** *48*, 10913-10925.

44. Solis, B. H.; Hammes-Schiffer, S., *J. Am. Chem. Soc.* **2012,** *134*, 15253-15256.

45. Heiden, Z. M.; Gorecki, B. J.; Rauchfuss, T. B., *Organometallics* **2008,** *27*, 1542-1549.

46. Corain, B.; Longato, B.; Favero, G.; Ajo, D.; Pilloni, G.; Russo, U.; Kreissl, F. R., *Inorg. Chim. Acta* **1989,** *157*, 259-266.

47. Pilloni, G.; Longato, B.; Corain, B., *J. Organomet. Chem.* **1991,** *420*, 57-65.

48. Barron, D.; Buti, S.; Ruiz, M.; Barbosa, J., *Phys. Chem. Chem. Phys.* **1999,** *1*, 295-298.

49. Felton, G. A. N.; Glass, R. S.; Lichtenberger, D. L.; Evans, D. H., *Inorg. Chem.* **2006,** *45*, 9181-9184.

50. Felton, G. A. N.; Vannucci, A. K.; Chen, J.; Lockett, L. T.; Okumura, N.; Petro, B. J.; Zakai, U. I.; Evans, D. H.; Glass, R. S.; Lichtenberger, D. L., *J. Am. Chem. Soc.* **2007,** *129*, 12521-12530.

51. Fourmond, V.; Jacques, P.-A.; Fontecave, M.; Artero, V., *Inorg. Chem.* **2010,** *49*, 10338-10347.

52. Helm, M. L.; Stewart, M. P.; Bullock, R. M.; DuBois, M. R.; DuBois, D. L., *Science* **2011,** *333*, 863-866.

53. Glassey, W. V.; Hoffmann, R., *J. Chem. Phys.* **2000,** *113*, 1698-1704.

54. Hoffmann, R., *Solids and Surfaces: A Chemist's View of Bonding in Extended Structures*. VCH Publishers: New York, 1988.

55. Gorelsky, S. I.; Lever, A. B. P., *J. Organomet. Chem.* **2001,** *635*, 187-196.

56. Ray, K.; Weyhermüller, T.; Neese, F.; Wieghardt, K., *Inorg. Chem.* **2005,** *44*, 5345-5360.

57. Ray, K.; Petrenko, T.; Wieghardt, K.; Neese, F., *Dalton Trans.* **2007**, 1552-1566.

58. Mutter, S. T.; Platts, J. A., *Chem-Eur. J.* **2010,** *16*, 5391-5399.

59. Liu, Y.-C.; Chu, K.-T.; Jhang, R.-L.; Lee, G.-H.; Chiang, M.-H., *Chem. Commun.* **2013,** *49*, 4743-4745.

60. Berggren, G.; Adamska, A.; Lambertz, C.; Simmons, T.; Esselborn, J.; Atta, M.; Gambarelli, S.; Mouesca, J. M.; Reijerse, E.; Lubitz, W.; Happe, T.; Artero, V.; Fontecave, M., *Nature* **2013,** *499*, 66-69.

61. Francl, M. M.; Pietro, W. J.; Hehre, W. J.; Binkley, J. S.; Gordon, M. S.; Defrees, D. J.; Pople, J. A., *J. Chem. Phys.* **1982,** *77*, 3654-3665.

62. Lee, C. T.; Yang, W. T.; Parr, R. G., *Phys. Rev. B* **1988,** *37*, 785-789.

63. Becke, A. D., *J. Chem. Phys.* **1993,** *98*, 5648-5652.

64. Stephens, P. J.; Devlin, F. J.; Chabalowski, C. F.; Frisch, M. J., *J. Phys. Chem.* **1994,** *98*, 11623-11627.

65. Rassolov, V. A.; Pople, J. A.; Ratner, M. A.; Windus, T. L., *J. Chem. Phys.* **1998,** *109*, 1223-1229.

66. Neese, F., *WIREs Comput. Mol. Sci.* **2012,** *2*, 73-78.

67. Harihara, P. C.; Pople, J. A., *Theoret. Chimica Acta* **1973,** *28*, 213-222.

68. Frisch, M. J.; Trucks, G. W.; Schlegel, H. B.; Scuseria, G. E.; Robb, M. A.; Cheeseman, J. R.; Montgomery Jr., J. A.; Vreven, T.; Kudin, K. N.; Burant, J. C.; Millam, J. M.; Iyengar, S. S.; Tomasi, J.; Barone, V.; Mennucci, B.; Cossi, M.; Scalmani, G.; Rega, N.; Persson, G. A.; Nakatsuji, H.; Hada, M.; Ehara, M.; Toyota, K.; Fukuda, R.; Hasegawa, J.; Ishida, M.; Niakajima, T.; Honda, Y.; Kitao, O.; Nakai, H.; Klene, M.; Li, X.; Konox, J. E.; Hratchian, H. P.; Cross, J. B.; Bakken, V.; Adamo, C.; Jaramillo, J.; Gomperts, R.; Stratmann, R. E.; Yazyev, O.; Austin, A. J.; Cammi, R.; Pomelli, C.; Ochterski, J. W.; Ayala, P. Y.; Morokuma, K.; Voth, G. A.; Salvador, P.; Dannenberg, J. J.; Zakrzewski, V. G.; Dapprich, S.; Daniels, A. D.; Strain, M. C.; Farkas, O.; Malick, D. K.; Rabuck, A. D.; Raghavachari, K.; Foresman, J. B.; Ortiz, J. V.; Cui, Q.; Baboul, A. G.; Clifford, S.; Cioslowski, J.; Stefanov, B. B.; Liu, G.; Liashenki, A.; Piskorz, P.; Komaromi, I.; Martin, R. L.; Fox, D. J.; Keith, T.; Al-Laham, M. A.; Peng, C. Y.; Nanayakkara, A.; Challacombe, M.; Gill, P. M. W.; Johnson, B.; Chen, W.; Wong, M. W.; Gonzalez, C.; Pople, J. A. *Gaussian 03, Revision C.02*, Gaussian, Inc. : Wallingford, CT, 2004.

69. Gorelsky, S. I. AOMix program, http://www.sg-chem.net/.

70. Tarakeshwar, P.; Finkelstein-Shapiro, D.; Hurst, S. J.; Rajh, T.; Mujica, V., *J. Phys. Chem. C* **2011,** *115*, 8994-9004.

71. Tarakeshwar, P.; Kumar, T. J. D.; Balakrishnan, N., *J. Phys. Chem. A* **2008,** *112*, 2846-2854.

72. Imbert, C.; Hratchian, H. P.; Lanznaster, M.; Heeg, M. J.; Hryhorczuk, L. M.; McGarvey, B. R.; Schlegel, H. B.; Verani, C. N., *Inorg. Chem.* **2005,** *44*, 7414-7422.

73. Greene, S. N.; Richards, N. G. J., *Inorg. Chem.* **2006,** *45*, 17-36.

74. Bruschi, M.; Zampella, G.; Fantucci, P.; De Gioia, L., *Coord. Chem. Rev.* **2005,** *249*, 1620-1640.

75. Ye, S. F.; Neese, F., *Inorg. Chem.* **2010,** *49*, 772-774.

76. Brothers, S. M.; Darensbourg, M. Y.; Hall, M. B., *Inorg. Chem.* **2011,** *50*, 8532-8540.

77. Wu, H.; Hall, M. B., *Comptes Rendus Chimie* **2008,** *11*, 790-804.

Figures

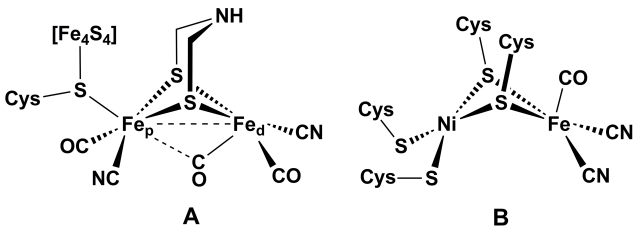

Figure 1. The active site of (A) [FeFe]-hydrogenase (H-cluster) and (B) [NiFe]-hydrogenase. Fe_d and Fe_p denote the distal and proximal iron, respectively, in the H-cluster.

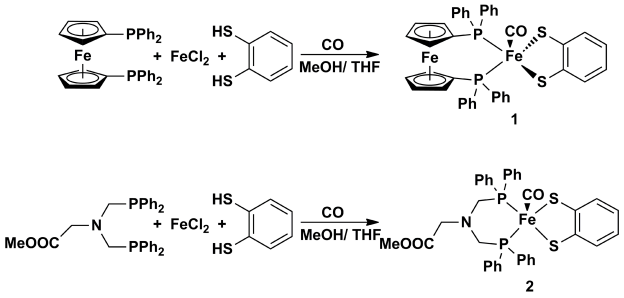

Scheme 1. Synthesis of complexes **1** and **2** from $FeCl_2$, the appropriate bis-phosphine ligand, benzene-1,2-dithiol, and CO.

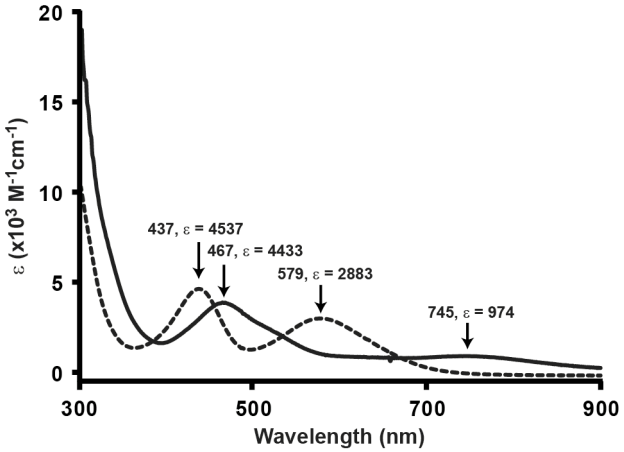

Figure 2. UV-vis spectra of **1** (solid line) and **2** (dashed line) in THF at room temperature. Spectra were collected from THF solutions of approximately 0.1 mM complex.

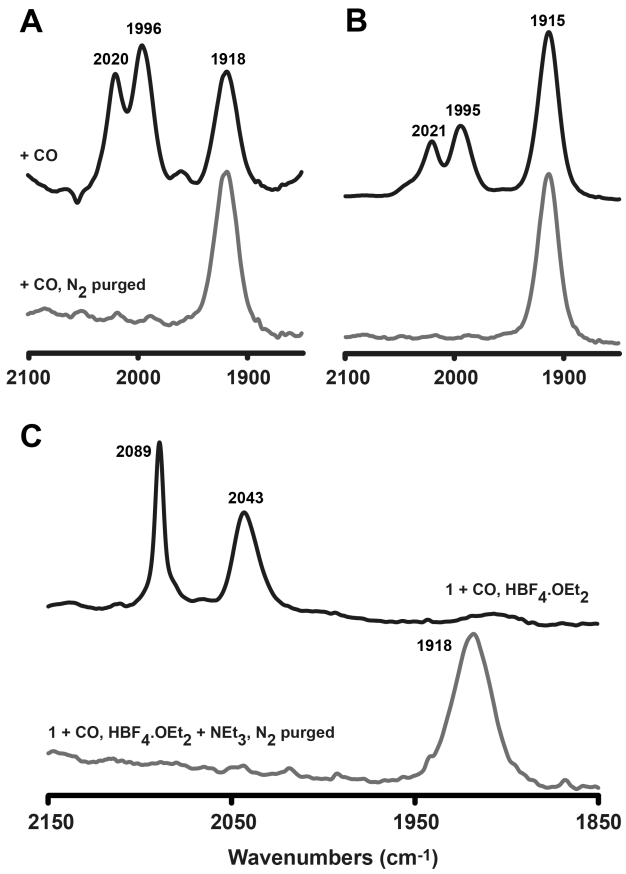

Figure 3. IR spectra in the presence and absence of CO for **1** (A) and **2** (B) in absence of acid. (C) Analogous spectra for **1** in the presence of 3 equiv. HBF_4. Black traces show the IR spectra after bubbling CO through the solutions of the complexes; Grey traces show the IR spectra after purging the solution with nitrogen to remove CO (A and B) and after addition of NEt_3 (C). Spectra were collected in CH_2Cl_2.

Table 1. Selected bond lengths (Å) and bond angles (˚) for **1** and **2**.

Bond lengths	**1**	**2**
Fe1-S1	2.1719(7)	2.2007(12)
Fe1-S2	2.2243(7)	2.1767(12)
Fe1-P1	2.2405(7)	2.2222(12)
Fe1-P2	2.2241(7)	2.2249(12)
Fe1-C41	1.732(3)	1.715(4)
C41-O41	1.162(3)	1.154(5)
Bond angles	**1**	**2**
P2-Fe-P1	101.18(2)	87.49(4)
S1-Fe1-S2	89.21(2)	89.31(4)
C41-Fe1-S1	134.57(8)	101.30(14)
C41-Fe1-S2	88.52(8)	106.58(14)
C41-Fe1-P1	90.19(8)	94.11(14)
C41-Fe1-P2	96.69(8)	93.28(14)
S1-Fe1-P2	128.48(3)	165.14(5)
S2-Fe1-P1	171.74(3)	159.2(5)
O1-C41-Fe1	173.4(2)	176.7(4)

Table 2. Bond distances (Å) within the benzene-1,2-dithiolate ligand in complexes **1** and **2**.

Bond lengths	**1**	**2**
C1-C6	1.398(3)	1.412(6)
C1-C2	1.404(3)	1.386(6)
C2-C3	1.410(3)	1.407(6)
C3-C4	1.365(3)	1.373(6)
C4-C5	1.401(4)	1.394(7)
C5-C6	1.380(3)	1.385(6)
C1-S1	1.745(2)	1.746(3)
C2-S2	1.735(2)	1.757(4)

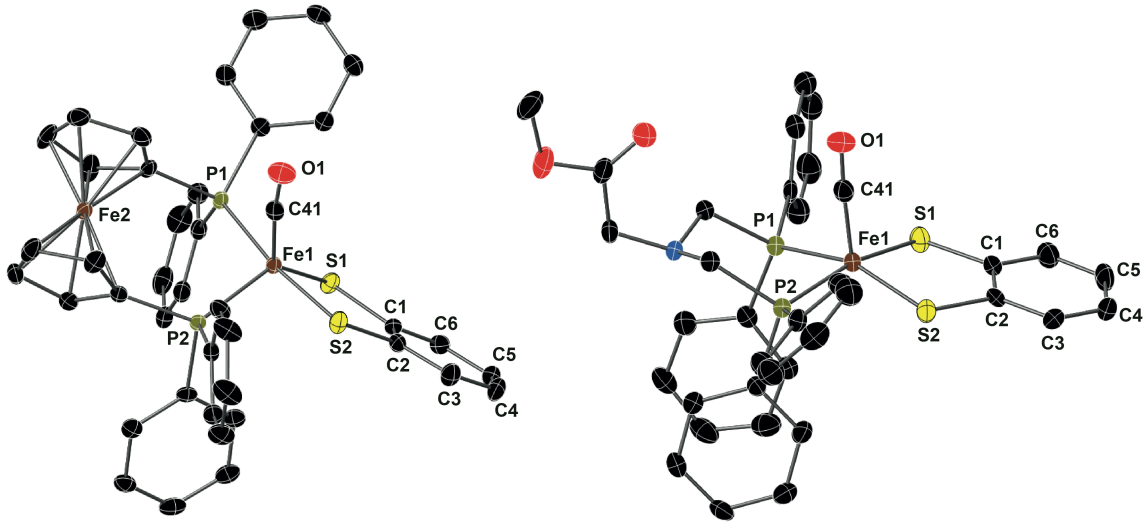

Figure 4. Molecular Structures of **1** (left) and **2** (right) with thermal ellipsoids drawn at 50% probability level; hydrogen atoms have been omitted for clarity.

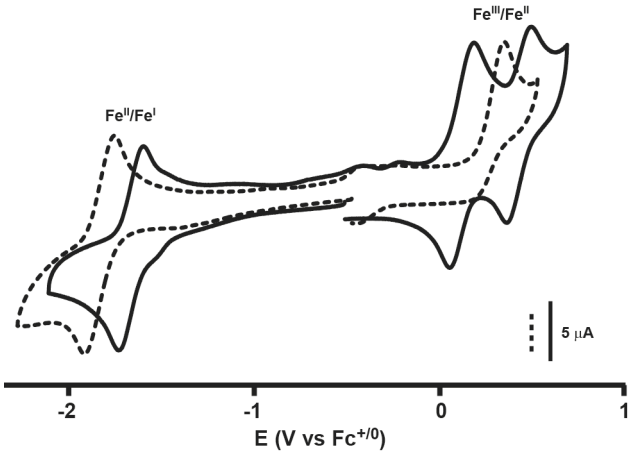

Figure 5. Cyclic voltammograms of **1** (solid line; 0.48 mM) and **2** (dashed line; 1.5 mM) in 0.1 M $[NBu_4][PF_6]$/ THF at a scan rate of 0.2 Vs^{-1}.

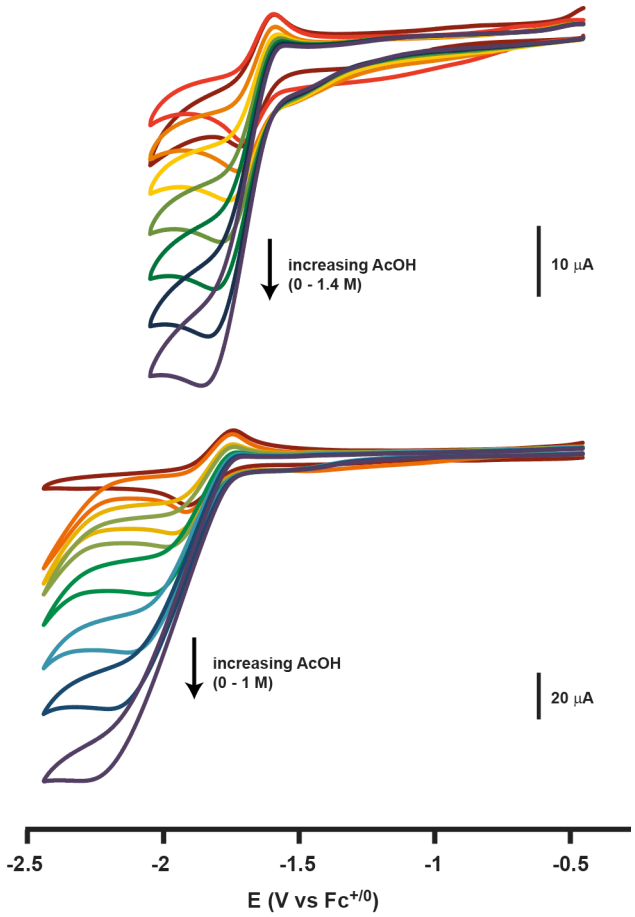

Figure 6. Cyclic voltammograms of **1** (top; 0.56 mM) and **2** (bottom; 1.25 mM) with various concentrations of acetic acid. The acid concentrations used are 0.2, 0.4, 0.6, 0.8, 1, 1.2, 1.4 M for complex **1** and 0.05, 0.1, 0.2, 0.4, 0.6, 0.8, 1 M for complex **2**. Other experimental conditions are as described in Figure 5.

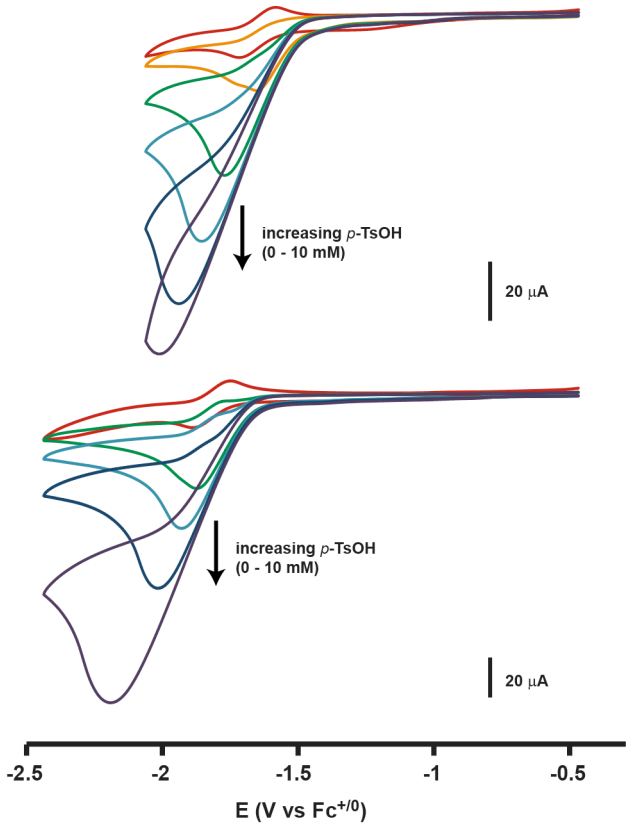

Figure 7. Cyclic voltammograms of **1** (top; 0.83 mM) and **2** (bottom; 0.88 mM) in the presence of *p*-TsOH. Acid concentrations are 2, 4, 6, 8, 10 mM for complex **1** and 1, 2, 3, 5, 10 mM for complex **2**. Other experimental conditions are as described in Figure 5.

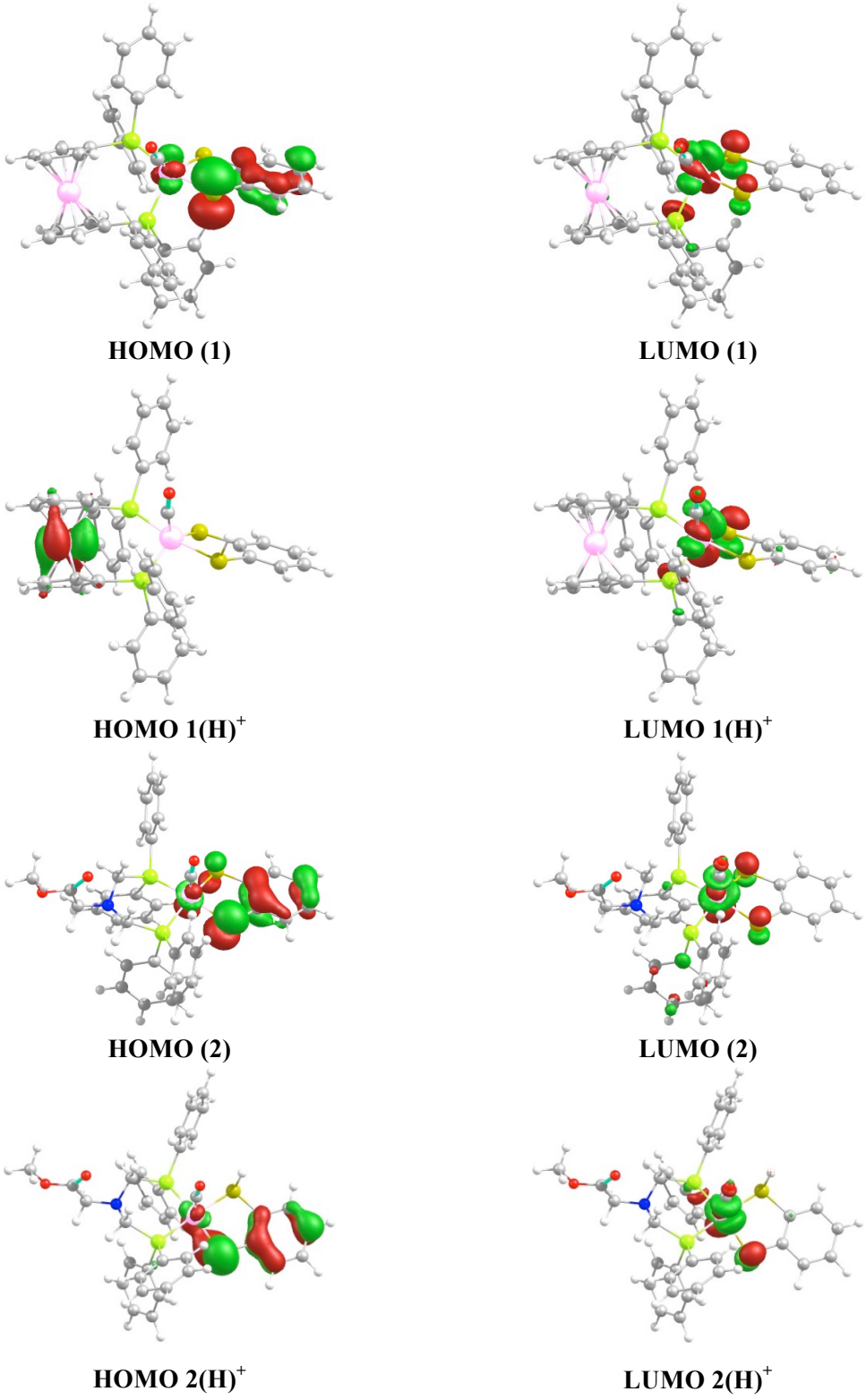

Figure 8. Electron density profiles of the HOMOs and LUMOs of **1**, **1(H)**$^+$, **2**, and **2(H)**$^+$.

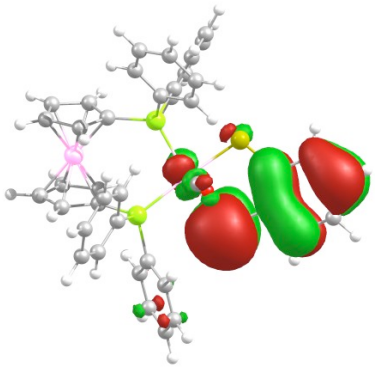

HOMO 1(H)-CO (TRANS)

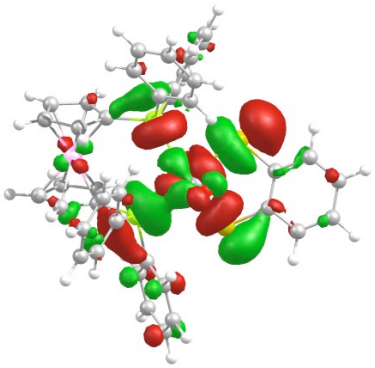

LUMO 1(H)-CO (TRANS)

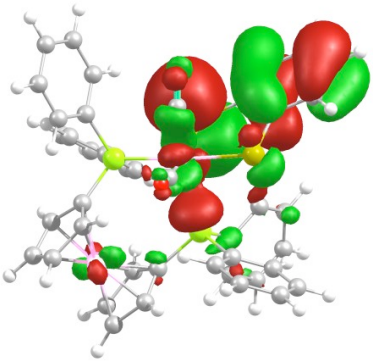

HOMO 1(H)-CO (CIS)

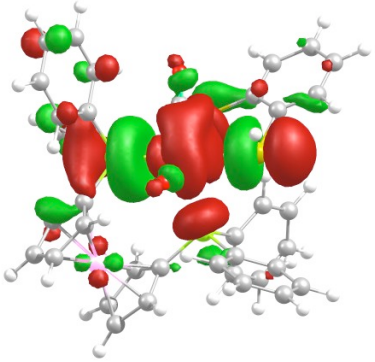

LUMO 1(H)-CO (CIS)

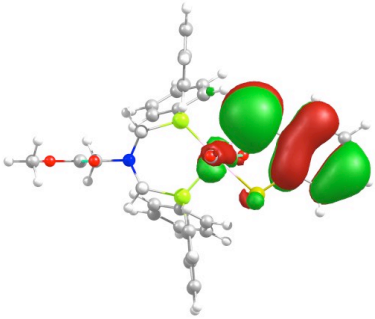

HOMO 2(H)-CO (TRANS)

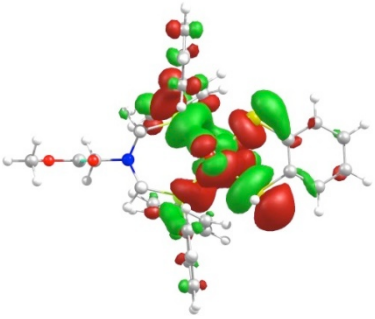

LUMO 2(H)-CO (TRANS)

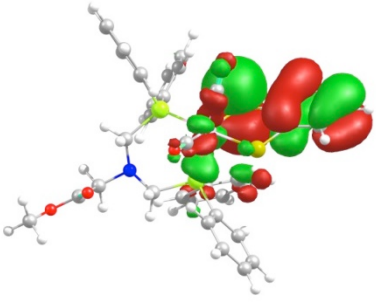

HOMO 2(H)-CO (CIS)

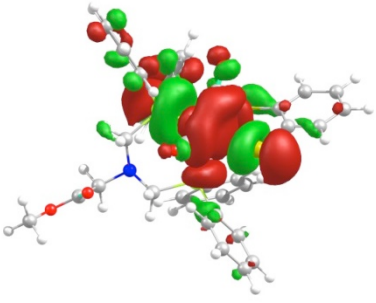

LUMO 2(H)-CO (CIS)

Figure 9: Electron density profiles of the HOMOs and LUMOs of the *cis* and *trans* conformers of [**1(H)-CO**]$^+$ and [**2(H)-CO**]$^+$.

For Table of Contents Only

Two chelating phosphine ligands have been used to prepare complexes of the form (bdt)Fe(CO)P_2 [bdt = benzene-1,2-dithiolate; P_2 = 1,1'-diphenylphosphinoferrocene (**1**) or methyl-2-{bis(diphenylphosphinomethyl)amino}acetate (**2**)] as models for the distal iron center in [FeFe]-hydrogenases. The geometric constraints of these two ligands leads to complexes with dramatically different coordination geometries: square planar and trigonal bipyramidal. These geometric differences are reflected in different reactivity towards protons and CO.